Three Reaction Pathways in the H + HCO → H_2 + CO Reaction†

Kurt M. Christoffel‡ and Joel M. Bowman*

Department of Chemistry and Cherry L. Emerson Center for Scientific Computation, Emory University, Atlanta, Georgia 30322

Received: November 30, 2008; Revised Manuscript Received: January 06, 2009

Ⓦ **This paper contains enhanced objects available on the Internet at http://pubs.acs.org/JPCA.**

We report quasiclassical trajectory calculations of the H + HCO → H_2 + CO reaction using a recent global potential energy surface. Three microscopic pathways are identified for this reaction. One is a direct abstraction, and the others both proceed via initial formation of a long-lived complex in the H_2CO well followed by reaction (a) over the molecular saddle point transition state or (b) via a roaming pathway previously identified for the unimolecular photodissociation reaction [Townsend et al., *Science* **2004**, *306*, 1158]. Cross sections and product internal energy distributions for each pathway are calculated for five initial collision energies.

1. Introduction

The reaction H + HCO → H_2 + CO has been the focus of several recent theoretical studies.[1−3] Harding and Wagner,[3] using limited ab initio calculations of the potential energy surface (PES), noted that direct abstraction was not only possible but was, according to their variational TST and RRKM calculations, the dominant pathway to the molecular products instead of the pathway via the deep H_2CO complex. More recently, Troe and Ushakov[2] performed classical trajectory calculations of this reaction, using a global ab initio-based potential energy surface,[4] and they concluded that about $^2/_3$ of the reaction proceeds via direct abstraction and $^1/_3$ via the H_2CO complex. The rate constant for this reaction has also been determined experimentally over a range of temperatures and pressures. (See ref 2 for a table of experimental results.) Calculations of the rate constant by Troe and Ushakov[2] are in excellent agreement with experiment, which indicates that this reaction is well characterized at the level of the thermal rate constant. Product state distributions of the H_2 and CO products with the same PES were examined in a very preliminary way by Rheinecker et al.[1] for zero impact parameter and one collision energy. They observed an interesting bimodal H_2 vibrational distribution and did note the two pathways mentioned above for this reaction. However, they did not quantify the branching between the two pathways, nor did they attempt to correlate this vibrational distribution with pathway.

In this paper we investigate the reaction dynamics in more detail and focus on the unexplored complex-forming pathway. Formation of the molecular products from the highly energized H_2CO complex has been studied both experimentally and theoretically in the context of photodissociation.[5] In these studies a "roaming" H-atom mechanism was reported in which the molecular products form via a pathway that bypasses the conventional molecular saddle-point transition state. The signature of this pathway is highly vibrationally excited H_2 and rotationally cold CO. On the basis of these results, it is of interest to determine the role of this pathway in the H + HCO reaction, and we do that in this paper. In the next section we discuss the computational details of the global ab initio potential energy surface, the QCT scattering calculations, and the metrics used to diagnose roaming. Our results are presented and discussed in section 3. In section 4, we summarize the important results of our work and conclude with an indication of directions for future study in systems where roaming is likely to play a significant dynamical role.

2. Computational Details

2.1. Potential Energy Surface. The formaldehyde PES used in this study is the full-dimensional ab initio-based S_0 surface developed by Zhang et al.[4] in 2004. This surface describes the isomers of formaldehyde (H_2CO and *cis*- and *trans*-HCOH), the pathways between these isomers, and the molecular (H_2 + CO) and radical (H + HCO) dissociation channels. Below we briefly describe this surface, particularly those features most relevant in the present study.

The H_2CO, HCOH, and H_2 + CO minima and the pathways connecting these minima are well described by a single-reference wave function and were treated at the CCSD(T) level of theory. Other inherently multireference regions, such as H + HCO and H + H + CO, were characterized via a multireference configuration interaction (MR-CI) approach. The ab initio calculations were performed with the MOLPRO software package[6] employing the Dunning augmented correlation consistent triple-ζ basis set.[7−9] The CCSD(T) calculations employed the closed-shell spin-restricted, coupled cluster theory (restricted to single and double excitations with perturbative triple excitations) of Hampel et al.[10] The MR-CI calculations employed the internally contracted, singles and doubles formalism of Werner and Knowles[11,12] with the orbitals used in the CI calculations optimized by complete active space, self-consistent field (CASSCF) methodology.

For these calculations, configuration space was divided into six overlapping regions: one centered on the formaldehyde isomers and their interconversion pathways, two centered on the H_2 + CO molecular dissociation channel, and three centered on the radical dissociation channels. Within each region, ab initio data at a large number of permutation symmetry-equivalent geometries were fit by use of a local fitting function. Generally this local fitting function was a finite direct product multinomial

† Part of the "George C. Schatz Festschrift".

* Corresponding author: e-mail joel.bowman@emory.edu.

‡ Permanent address: Department of Chemistry, Augustana College, Rock Island, IL 61201-2296.

10.1021/jp810517e CCC: $40.75
Published on Web 02/23/2009

in Morse variables for the six internuclear distances R_{CHa}, R_{CHb}, R_{CO}, R_{OHa}, R_{OHb}, and R_{HH}, denoted simply as r_1-r_6, respectively, given by

$$V(r_1, ..., r_6) = \sum_{n_1,...,n_6} C_{n_1,...,n_6} \prod_{i=1}^{6} [1 - e^{-\alpha(r_i - r_{ie})}]^{n_i} \quad (1)$$

where α was set to $0.5/a_0$; r_{ie} are the equilibrium internuclear distances at the formaldehyde global minimum geometry; and the sum of the powers n_i was restricted to be less than or equal to 6. A total of over 60 000 symmetry-unique ab initio points were used in the six regions. These six local fits were joined by use of five switching functions (described in detail in ref 4) to generate a single global potential energy surface.

On this fitted PES, the floor of the asymptotic H + HCO channel lies 33 239 cm^{-1} above the formaldehyde global minimum. No barrier occurs along the minimum energy path (MEP) from H_2CO to H + HCO. The difference in harmonic zero-point energy between H + HCO and H_2CO is −2989 cm^{-1}, which yields an approximate D_0 value for this channel of 30 250 cm^{-1}, which is within 100 cm^{-1} of experimental estimates.[13,14] The H_2 + CO minimum lies 1931 cm^{-1} above the global minimum, in good agreement with the best calculated D_e value of 2028 cm^{-1}.[15] Along the MEP between these two minima, a saddle point occurs with an energy 30 584 cm^{-1} above the H_2CO global minimum in good agreement with the best ab initio value of 30 683 cm^{-1}.[15] This saddle point (designated TS_3 in earlier work) corresponds to a planar skewed configuration with both hydrogens to one side of the C−O axis. This surface then appears to give a good description of both the radical and molecular dissociation channels. It has been used in several theoretical studies of H_2CO photodissociation and found to produce results in semiquantitative agreement with experiment.[1,5,16−21]

2.2. Quasiclassical Trajectory Scattering Calculations. Quasiclassical trajectory (QCT) calculations were performed for five values of relative translational energy E_{trans} (0.01, 0.025, 0.05, 0.10, and 0.20 eV) for the purpose of obtaining collision cross sections and product state distributions for the three reaction pathways discussed above. In production runs to obtain the reaction cross section at each E_{trans} value, batches of 5000 trajectories were integrated per impact parameter b, ranging from 0 to b_{max}, where b_{max} is the maximum impact parameter for which reaction occurs. For this system with an entrance channel exhibiting no barrier, b_{max} fell off with increasing E_{trans}, ranging from $12a_0$ at E_{trans} = 0.01 eV to $8.5a_0$ at E_{trans} = 0.20 eV. Typically reaction probabilities for fixed impact parameter for each of the three pathways $P_i(b, E_{trans})$ (where i = D for direct reaction, TS for addition followed by reaction via the transition state, or R for addition followed by reaction via a roaming mechanism) were calculated every $0.5a_0$ except near b_{max}, where they were calculated with a spacing of $0.25a_0$. Cross sections were then obtained by numerically evaluating the integral

$$\sigma_i(E_{trans}) = 2\pi \int_0^{b_{max}+0.25a_0} P_i(b, E_{trans}) b \, db \quad (2)$$

All trajectories were initiated with HCO internal coordinates and momenta associated with the "quasiclassical state" corresponding to the quantum ground rovibrational state. The initial total angular momentum of HCO was set to 0, and a normal-mode description was assumed for the vibrational ground state. Normal-mode amplitudes were assigned as $A_i = (\hbar/\omega_i)^{1/2}$, where ω_i is the normal-mode frequency. Normal-mode phases were selected randomly and the normal-mode coordinates and velocities were determined from well-known results. The corresponding Cartesian coordinates and velocities were obtained by standard linear transformation. [22]

Quasiclassical rotational and vibrational quantum numbers were determined for the H_2 and CO products. The space-fixed Cartesian coordinates and momenta at the termination of a reactive trajectory were used to calculate the rotational angular momentum and the rovibrational energy of each diatomic product. The rotational quantum number j is determined from the classical rotational angular momentum J by $J = [j(j+1)\hbar]^{1/2}$. The continuous quantity j was "binned" in the standard manner to make an integer quasiclassical product rotational state assignment. To assign vibrational quantum numbers v to the diatomics, tables of quantum rovibrational energies were first obtained by numerical solution of the exact rovibrational Schrödinger equation:

$$\left[-\frac{\hbar^2}{2\mu}\frac{d^2}{dr^2} + \frac{j(j+1)\hbar^2}{2\mu r^2} + V_{BC}(r) - E_{vj}\right]\varphi_{vj}(r) = 0 \quad (3)$$

where j is an integer rotational quantum number of H_2 or CO and V_{BC} is the potential energy of H_2 or CO. Then a vibrational quantum number v is assigned by finding the rovibrational eigenvalue E_{vj} closest to the classical rovibrational energy for the given (rounded, i.e., integer) j determined first as described above.

All trajectories started with a $14a_0$ separation between the H atom and the center of mass of HCO with the orientation of HCO randomly selected. The equations of motion were integrated via a sixth-order Adams−Moulton method with a time step of 5 atu (approximately 0.12 fs). This step size was sufficient to ensure conservation of energy to six significant figures for the vast majority of trajectories despite the prevalence of long-lived collision complexes (highly excited H_2CO) at all the energies considered here. [At each energy, the small number of trajectories for which energy conservation was inadequate were discarded.] The trajectories were then integrated until products had again separated to a distance of $14a_0$ or a maximum number of integration steps, N_{max}, had been exceeded. As discussed below, we settled on an N_{max} value of 250 000 as a compromise between computational expense and a desire to obtain the maximum number of completed trajectories.

2.3. Metrics for Complex Formation and Roaming. Given the large number of trajectories (in excess of a half-million) required here to obtain the reaction cross sections and product distributions, it was imperative that we devise relatively simple metrics to distinguish direct reactive trajectories from trajectories that become temporarily trapped in the H_2CO complex region, and within this latter class of trajectories, to easily distinguish between those that react via the transition-state region from those that react via a roaming mechanism. In the preliminary stages of this investigation we examined the lifetime distribution (at a fixed value of E_{trans}) for reactive trajectories. Figure 1 shows the short-time part of the distribution of reactive lifetimes in histogram form for a batch of 100 000 trajectories (that samples the full range of impact parameters from 0 to $12a_0$ and gives 42 175 reactive trajectories) for E_{trans} = 0.01 eV. Clearly a majority of all reactive trajectories at this energy fall into the second and third bins (corresponding to trajectory durations of 30 000 atu or less). In fact these two bins contain 29 320 trajectories, corresponding to 69.5% of all reactive trajectories, in good agreement with the estimate by Troe and Ushakov[2] that $^2/_3$ of the reaction proceeds via a direct abstraction mechanism. On the basis of this and other similar evidence (at other E_{trans} values) we adopted energy-dependent lifetime limits for a reactive trajectory to be classified as direct. These limits ranged

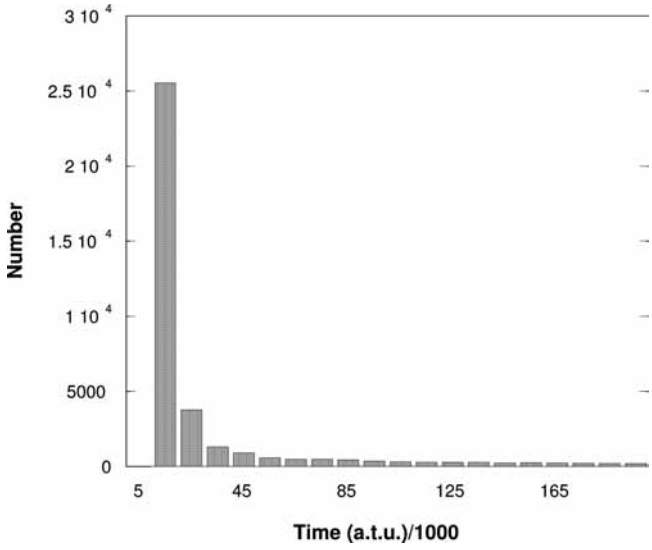

Figure 1. Histogram representation of short-time detail of reactive event lifetime distribution for $E_{trans} = 0.01$ eV.

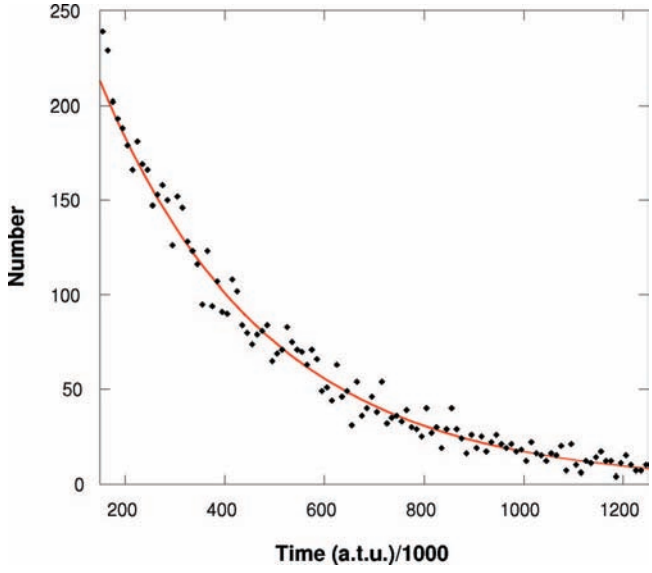

Figure 2. Long-time detail of reactive event lifetime distribution for $E_{trans} = 0.01$ eV.

from 30 000 atu for $E_{trans} = 0.01$ eV down to 15 000 atu for $E_{trans} = 0.20$ eV. Generally this limit was approximately 2.5 times the duration of the shortest direct reactive trajectory at that energy. At each value of E_{trans}, trajectories with durations that exceeded the corresponding energy-specific direct limit were considered to have formed a collision complex. Figure 2 shows a long-time detail of the lifetime distribution shown in Figure 1. It can be seen there that, in the long-time limit, the lifetime distribution is well described by an exponential fit. It is this long-time exponential character of the lifetime distribution that renders it impractical to attempt to integrate all trajectories to completion.

Among the long-lived trajectories, we must further distinguish between transition-state trajectories that pass through/near TS_3 to reach the molecular product channel and roaming trajectories. In previous work on formaldehyde photodissociation, trajectories producing the molecular products were classified as roaming on the basis of detailed analysis of individual trajectories in terms of the temporal behavior of internuclear distances.[16,19,21]

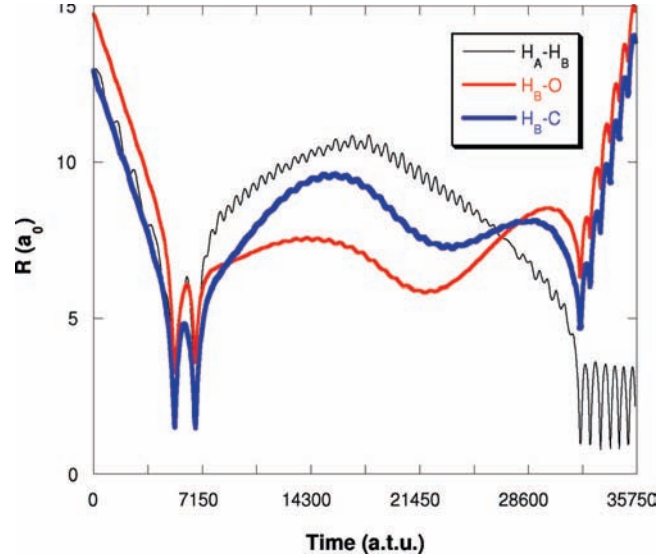

Figure 3. Time dependence of selected internuclear distances for a roaming trajectory ($b = 8a_0$, $E_{trans} = 0.05$ eV).

Figure 3 shows a plot of time evolution of the distances of incoming hydrogen atom H_B from the three atoms of HCO for what might be termed an extreme roaming trajectory (at $E_{trans} = 0.05$ eV and $b = 8a_0$) that gives rise to molecular products. It can be seen there that an H_2CO complex forms about 5000 atu into this trajectory, and the system then appears to be headed toward the H + HCO products shortly after 7000 atu, as indicated by the large and growing separation of H_B from the other three atoms for approximately the next 10 000 atu. However, H_B then closes the distance with HCO until near 32 000 atu, when H_B approaches close enough to H_A in HCO to abstract it in an essentially intramolecular manner.

Although such analysis provides great insight into the nature of the roaming mechanism, it does not lend itself to a simple metric for characterizing long-lived reactive trajectories as roaming or transition state. Our development of such a metric for this study was guided by two observations: (1) Roaming trajectories skirt or bypass the transition state.[23] (2) Prior studies of formaldehyde photodissociation show that roaming events favored formation of highly vibrationally excited H_2 (as can be seen in Figure 3) and rotationally cold CO, while long-lived transition-state trajectories resulted in substantially lower levels of H_2 vibrational excitation and substantially higher levels of CO rotational excitation.[5,16,18−21] As a result, in the early stages of this work we studied the time dependence of the root-mean-square deviation (RMSD) of the system geometry from the transition state (TS_3) geometry for large numbers of both types of long-lived reactive trajectories. In terms of the six internuclear distances:

$$\mathrm{RMSD}(t) = \sqrt{\frac{\sum_{i=1}^{6} (r_i - r_{i,\mathrm{TS}_3})^2}{6}} \qquad (4)$$

We observed a very strong correlation between the type of trajectory and the value of RMSD(t) at the last point of nearest approach to TS_3 prior to reaction and separation [a local minimum in RMSD(t) versus time]. Figure 4 shows an example of typical RMSD(t) (at last point of nearest approach) distributions for long-lived trajectories that clearly pass through/near TS_3 and for clearly roaming trajectories. As seen there (and as

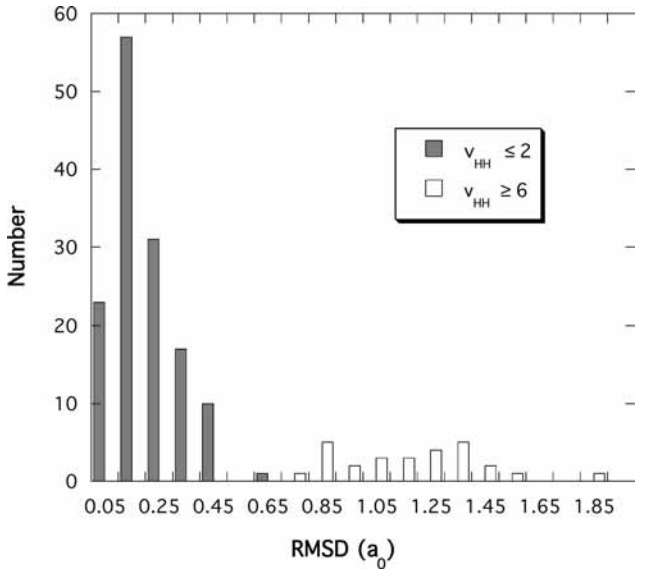

Figure 4. Distribution of RMSD(t) values for collision complex-forming trajectories ($b = 8a_0$, $E_{trans} = 0.05$ eV).

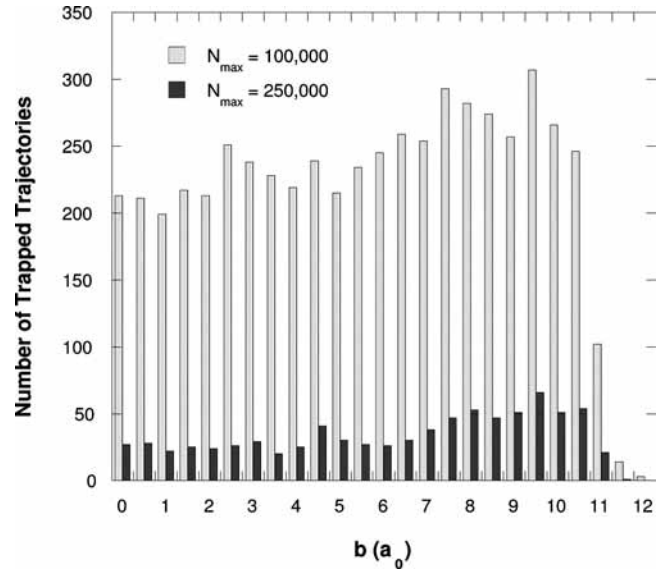

Figure 5. Incidence of incomplete/trapped trajectories for two values of N_{max} at $E_{trans} = 0.05$ eV versus impact parameter b (4000 total trajectories run at each b value).

we saw in a great many similar plots), there is a clean break in RMSD values between the two types of trajectories. On the basis of this empirical evidence, we decided on the following simple diagnostic to distinguish transition-state trajectories from roaming trajectories in terms of the value of RMSD(t) at its local minimum immediately prior to product separation. Transition-state trajectories are characterized by an RMSD(t) value less than $0.7a_0$, while roaming trajectories are those for which RMSD(t) $\geq 0.7a_0$.

Although our metrics for trajectory classification are somewhat arbitrary, they are based on extensive empirical data. The tradeoff for their simplicity is the possibility of seepage between categories (due to incorrect assignments). However, we feel that our metrics are sufficiently clean that the results reported in section 3 below are at least semiquantitatively correct.

3. Results and Discussion

3.1. Reaction Cross Sections. One of the primary goals of this work was to determine the relative contributions of the three pathways in this system to the overall reactivity. For this purpose, collision cross sections for each of these pathways were calculated at five values of the relative translational energy E_{trans} (0.01, 0.025, 0.05, 0.10, and 0.20 eV). As discussed earlier, the presence of the deep H_2CO well on the PES and the resultant significant number of long-lived trajectories present a computational impediment to the calculation of collision cross sections. This problem is particularly acute at the lowest E_{trans} value considered here. Initially we set an upper limit on N_{max} of 100 000, based on earlier studies of H_2CO photodissociation.[5,17] It quickly became apparent that this resulted in an unacceptably high number of incomplete trajectories. Figure 5 shows the number of incomplete (i.e., trapped in the H_2CO or HCOH isomeric wells) trajectories for batches of 4000 trajectories run with $E_{trans} = 0.01$ eV and N_{max} values of 100 000 or 250 000 versus impact parameter. For $N_{max} = 100\,000$, the number of trapped trajectories is typically 200−300 (representing about 5−7% of the total) except for impact parameters very close to b_{max}, where the occurrence of complex formation falls off precipitously. However, at this energy for N_{max} equal to 100 000, the typical number of trapped trajectories is comparable in magnitude to the number of trajectories identified as roaming or as transition state. Any reactive trajectories among these trapped trajectories, if integrated to completion, would fall into the transition-state or roaming categories. Thus a calculation of $P_i(b, E_{trans})$ in eq 2 based on completed trajectories is biased against the two pathways that occur via complex formation to an extent that increases with the prevalence of incomplete/trapped trajectories. As a result, we ultimately increased the maximum number of integration steps to 250 000. As can be seen in Figure 5, increasing N_{max} from 100 000 to 250 000 typically has the effect of reducing the number of trapped trajectories by a factor of 5−10. Undoubtedly the number and significance of trapped trajectories could be further reduced by further increases in the value of N_{max}, but due to the long-time exponential character of the lifetime distribution, we judged that the slight improvement in statistics that might be gained did not justify the dramatic increase in computational resources required.

Table 1 shows the effect of trapped trajectories by comparing at three relative translational energies computed cross sections (using the same 4000 trajectories per impact parameter) for calculations using N_{max} values of 100 000 and 250 000. As can be seen, the total cross sections are relatively insensitive to the choice of N_{max}, differing by less than 1.5% in all three cases. However, both absolute and relative changes in the roaming and transition-state cross sections tend to be more pronounced. This underscores again the importance of reducing, as far as practical, the number of trapped trajectories in these calculations. It should also be noted from Table 1 that reducing the number of trapped trajectories by increasing N_{max} has the effect of increasing the computed values of σ_R and σ_{TS} while decreasing the computed value of σ_D. Thus, our results that are still based on QCT calculations from which trapped trajectories have not been completely eliminated should be viewed as giving lower bounds on σ_R and σ_{TS} while giving an upper bound on σ_D.

Figure 6 shows our best (using 5000 trajectories per impact parameter and $N_{max} = 250\,000$) computed cross sections (total and for the three pathways) versus E_{trans}. As seen, all four cross sections fall off with increasing E_{trans} (typical behavior for a barrierless reaction) in a manner that is well-described by a power law decay of the form $\sigma_i = A_i E_{trans}^{-p_i}$. The p_i values for σ_{tot}, σ_D, and σ_{TS} are all very similar and lie near 0.4. The roaming

TABLE 1: Effect of N_{max} on Reactive Cross Sections (a_0^2)

	E_{trans} = 0.01 eV		E_{trans} = 0.05 eV		E_{trans} = 0.10 eV	
	N_{max} = 100 000	N_{max} = 250 000	N_{max} = 100 000	N_{max} = 250 000	N_{max} = 100 000	N_{max} = 250 000
σ_R	19.05	19.44	3.64	4.03	2.39	2.69
σ_{TS}	28.00	35.32	16.48	19.90	12.39	14.45
σ_D	129.94	123.44	68.78	66.15	52.84	51.15
σ_{tot}	176.99	178.20	88.89	90.08	67.62	68.29

TABLE 2: Comparison of Relative Cross Sections versus Relative Translational Energy E_{trans}

E_{trans} (eV)	$(\sigma_R + \sigma_{TS})/\sigma_{tot}$	σ_R/σ_{TS}	σ_R/σ_{tot}
0.01	0.313	0.558	0.112
0.025	0.279	0.249	0.0556
0.05	0.275	0.214	0.0484
0.10	0.262	0.216	0.0464
0.20	0.244	0.216	0.0433

cross section shows a more abrupt fall-off with increasing E_{trans}, characterized by a p value near 0.7. Table 2 presents a relative comparison of the various cross sections for the five E_{trans} values. The data presented there clearly indicate that the relative contribution of the two pathways involving a collision complex intermediate [as measured by the ratio $(\sigma_R + \sigma_{TS})/\sigma_{tot}$] exhibits a slow but steady decline with increasing E_{trans}. The relative contribution of the roaming pathway (as measured by σ_R/σ_{TS} and σ_R/σ_{tot}) falls off quickly between the lowest two E_{trans} values but more gradually as E_{trans} is increased further. In fact, when measured as a fraction of σ_{TS} for the three largest E_{trans} values, σ_R is essentially constant.

3.2. Product State Distributions. The second major goal of this study was to determine whether or not the three pathways for the title reaction exhibited distinctive product state distribution signatures. For this purpose, we calculated for each diatomic fragment and for each pathway final vibrational state-specific (summed over all rotational states of that fragment and over all rovibrational states of the other fragment) and final rotational state-specific (summed over all vibrational states of that fragment and over all rovibrational states of the other fragment) cross sections for the diatomic molecular products. Figure 7 shows vibrational state distributions for molecular hydrogen for the three pathways with E_{trans} = 0.01 eV. [Here we limit our figures to E_{trans} = 0.01 eV, where we have the most reactive events for binning and hence the best statistics. Also, the distributions are relatively insensitive to E_{trans}, and those at the higher E_{trans} values considered here are qualitatively similar to the E_{trans} = 0.01 eV results.] It can be seen there that the direct abstraction pathway favors a high level of H_2 vibrational excitation with a peak at v = 7. The H_2 vibrational state distribution for the roaming (intramolecular abstraction) pathway is similar to that for the direct pathway (although obviously contributing much less to the overall reaction cross section) with peaks at 6 and 7. The transition-state H_2 vibrational state distribution is dramatically different, peaking at 0 and 1 and rapidly falling off with increasing v. The distributions seen for the roaming and transition-state pathways are qualitatively consistent with those seen in earlier studies of formaldehyde photodissociation.[5,16,17,19]

Figure 8 shows the corresponding H_2 rotational state distributions. Here compared to the vibrational distributions shown in Figure 7, the differences between the three pathways are relatively minor. All cover a relatively broad range of j_{H_2}values and all peak at relatively modest amounts of rotational excitation (j_{H_2} in the range 3−6). The transition-state distribution is somewhat narrower and peaks at a slightly lower j_{H_2} value than the other two distributions.

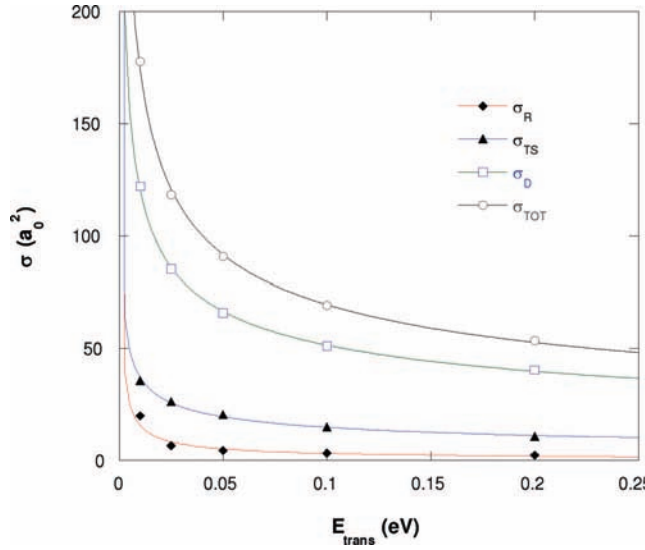

Figure 6. Relative translational energy dependence of reaction cross sections.

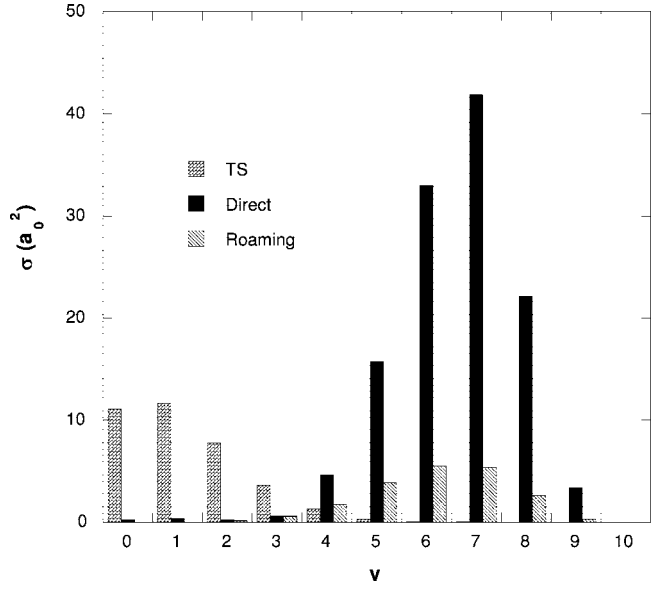

Figure 7. Cross sections to form product H_2 in indicated vibrational state v, plotted versus v (E_{trans} = 0.01 eV).

Figures 9 and 10 show the final vibrational and rotational state distributions, respectively, for the CO product. As can be seen in Figure 9, for all three pathways the vibrational distributions are qualitatively quite similar, in all cases corresponding to very minimal excitation of the C−O stretching motion. In all three cases the v_{CO} = 0 channel accounts for over 70% of the total cross section; for the two pathways that proceed via collision complex formation, this number is even higher, over 80%. Events producing carbon monoxide assigned to quasiclassical states with $v_{CO} \geq 2$

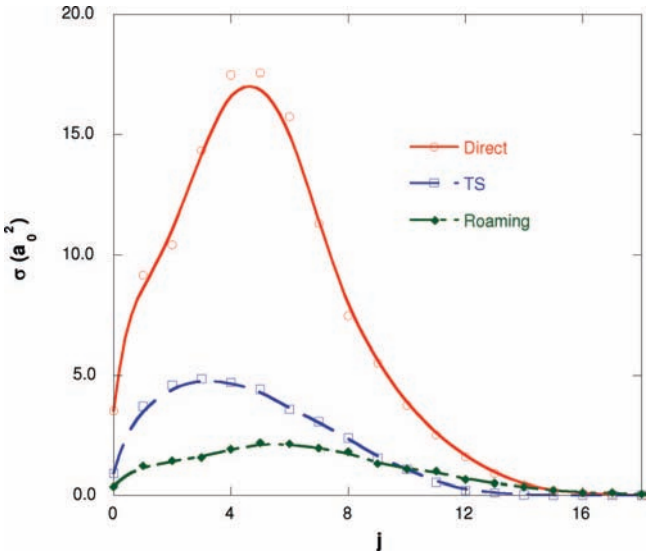

Figure 8. Cross sections to form product H_2 in indicated rotational state j, plotted versus j (E_{trans} = 0.01 eV).

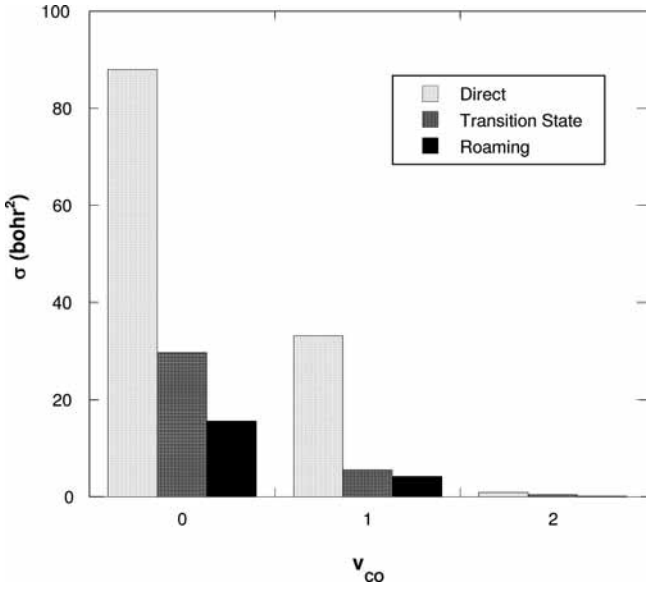

Figure 9. Cross sections to form product CO in indicated vibrational state v, plotted versus v (E_{trans} = 0.01 eV).

account for less than 1% of the total reactive cross section. Thus it appears that, to a good approximation, the C−O stretching motion is a spectator mode in this reaction. In sharp contrast, Figure 10 shows marked differences between the CO rotational state distributions for the three pathways. All three distributions are relatively broad, spreading over 30−40 j_{CO} values with appreciable amplitude. For the direct and roaming pathways, the distributions peak at low j_{CO} values (between 5 and 10) and fall off gradually, with negligible contributions from j_{CO} values above 40. The transition-state distribution has a relatively flat plateau between j_{CO} = 34 and j_{CO} = 48 and falls off to become insignificant for j_{CO} < 15 and j_{CO} > 65. Thus the transition-state distribution is largest for j_{CO} values where the other two distributions are rapidly approaching zero amplitude. The direct and roaming distributions peak at j_{CO} values that are essentially unpopulated by the transition-state pathway.

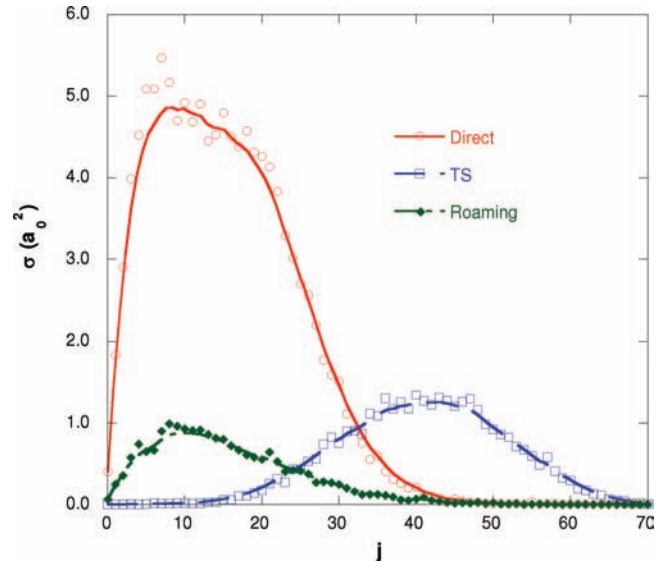

Figure 10. Cross sections to form product CO in indicated rotational state j, plotted versus j (E_{trans} = 0.01 eV).

4. Summary and Conclusions

We have shown that three pathways— direct abstraction and collision complex formation followed by either transition-state-mediated or roaming dynamics—play significant roles in the H + HCO → H_2 + CO reaction at relative translational energies, E_{trans}, as high as 0.20 eV. Overall reactivity and the relative contributions of the roaming and transition-state pathways decrease as E_{trans} increases. The direct and roaming pathways were correlated with a high level of H_2 vibrational excitation and a low level of CO rotational excitation. The transition-state pathway was correlated with low levels of H_2 vibrational excitation and high levels of CO rotational excitation. All three pathways produced very little CO vibrational excitation and modest H_2 rotational excitation.

Multiple pathway mechanisms in chemical reactions are not uncommon. Earlier theoretical and experimental work on the CH_3 + O reaction supported the existence of two pathways to CO product.[24] One of these followed a stepwise minimum-energy pathway involving first CH bond cleavage in the methoxy radical, forming H + H_2CO, followed by an abstraction, forming H_2 + HCO. However, at the energies considered in that work, a second pathway (that bypasses the MEP) involving direct abstraction of H_2 from the methoxy radical became significant. In both cases, subsequent fragmentation of the HCO radical produced the CO product. Work on the bimolecular H + HBr[25] and H + CH_4 reactions[26−28] at high energies found that these reactions proceed by pathways that deviate substantially from the conventional transition-state pathway. Recently a roaming mechanism that bypasses the MEP transition state has been postulated to explain bimodal product state distributions seen in the photodissociations of acetaldehyde[29] and acetone.[30] Bowman and co-workers[31,32] have used a new ab initio full-dimensional PES for the acetaldehyde system and QCT calculations to confirm that non-transition-state dynamics are significant there. Thus it appears that roaming or other pathways that bypass the transition state may be commonplace. Work in this laboratory continues into the role of such dynamics in the formaldehyde and acetaldehyde systems.

Finally, we have recorded sample animations of direct and roaming trajectories for the present reaction.

Acknowledgment. Financial support from the Department of Energy (DE-FG02-97ER14782) is gratefully acknowledged.

References and Notes

(1) Rheinecker, J. L.; Zhang, X.; Bowman, J. M. *Mol. Phys.* **2005**, *103*, 1067.

(2) Troe, J.; Ushakov, V. *J. Phys. Chem. A* **2007**, *111*, 6610.

(3) Harding, L. B.; Wagner, A. F. *Proc. Combust. Inst.* **1986**, *21*, 721.

(4) Zhang, X.; Zou, S.; Harding, L. B.; Bowman, J. M. *J. Phys. Chem. A* **2004**, *108*, 8980.

(5) Zhang, X.; Rheinecker, J. L.; Bowman, J. M. *J. Chem. Phys.* **2005**, *122*, 114313.

(6) MOLPRO is a package of ab initio programs written by H.-J. Werner and P. J. Knowles, with contributions from J. Almlof, R. D. Amos, A. Berning, D. L. Cooper, M. J. O. Deegan, A. J. Dobbyn, F. Eckert, S. T. Elbert, C. Hampel, R. Lindh, A. W. Lloyd, W. Meyer , A. Nicklass, K. Peterson, R. Pitzer, A. J. Stone, P. R. Taylor, M. E. Mura, P. Pulay, M. Schutz, H. Stoll, and T. Thorsteinsson.

(7) Dunning, T. H., Jr. *J. Chem. Phys.* **1989**, *90*, 1007.

(8) Kendall, R. A.; Dunning, T. H., Jr.; Harrison, R. J. *J. Chem. Phys.* **1992**, *96*, 6796.

(9) Woon, D. E.; Dunning, T. J., Jr. *J. Chem. Phys.* **1993**, *98*, 1358.

(10) Hampel, C.; Peterson, K.; Werner, H.-J. *Chem. Phys. Lett.* **1992**, *190*, 1.

(11) Werner, H.-J.; Knowles, P. J. *J. Chem. Phys.* **1988**, *89*, 5803.

(12) Knowles, P. J.; Werner, H.-J. *Chem. Phys. Lett.* **1988**, *145*, 514.

(13) Terentis, A. C.; Kable, S. H. *Chem. Phys. Lett.* **1996**, *258*, 626.

(14) Chuang, M.; Foltz, M. F.; Moore, C. B. *J. Chem. Phys.* **1987**, *87*, 3855.

(15) Feller, D.; Dupuis, M.; Garrett, B. C. *J. Chem. Phys.* **2000**, *113*, 218.

(16) Townsend, D.; Lahankar, S. A.; Lee, S. K.; Chambreau, S. D.; Suits, A. G.; Zhang, X.; Rheinecker, J.; Harding, L. B.; Bowman, J. M. *Science* **2004**, *306*, 1158.

(17) Bowman, J. M.; Zhang, X. *Phys. Chem. Chem. Phys.* **2006**, *8*, 321.

(18) Yin, H. M.; Kable, S. H.; Zhang, X.; Bowman, J. M. *Science* **2006**, *311*, 1443.

(19) Lahankar, S. A.; Chambreau, S. D.; Townsend, D.; Suits, F.; Farnum, J; Zhang, X.; Bowman, J. M.; Suits, A. G. *J. Chem. Phys.* **2006**, *125*, 044303.

(20) Lahankar, S. A.; Chambreau, S. D.; Zhang, X.; Bowman, J. M.; Suits, A. G. *J. Chem. Phys.* **2007**, *126*, 044314.

(21) Lahankar, S. A.; Goncharov, V.; Suits, F.; Farnum, J. D.; Bowman, J. M.; Suits, A. G. *Chem. Phys.* **2008**, *347*, 288.

(22) Wilson, E. B.; Decius, J. C.; Cross, P. C. *Molecular Vibrations*; Dover Publications: New York, 1980.

(23) Bowman, J. M. *Proc. Natl. Acad. Sci. U.S.A.* **2006**, *103*, 16061.

(24) Marcy, T. P.; Díaz, R. R.; Heard, D.; Leone, S. R.; Harding, L. B.; Klippenstein, S. J. *J. Phys. Chem. A* **2001**, *105*, 8361.

(25) Pomerantz, A. E.; Camden, J. P.; Chiou, A. S.; Ausfelder, F.; Chawla, N.; Hase, W. L.; Zare, R. N. *J. Am. Chem. Soc.* **2005**, *127*, 16368.

(26) Camden, J. P.; Hu, W.; Bechtel, H. A.; Brown, D. J. A.; Martin, M. R.; Zare, R. N.; Lendvay, G.; Troya, D.; Schatz, G. C. *J. Phys. Chem. A* **2006**, *110*, 677.

(27) Hu, W.; Lendvay, G.; Troya, D.; Schatz, G. C.; Camden, J. P.; Bechtel, H. A.; Brown, D. J. A.; Martin, M. R.; Zare, R. N. *J. Phys. Chem. A* **2006**, *110*, 3017.

(28) Xie, Z.; Bowman, J. M. *Chem. Phys. Lett.* **2006**, *429*, 355.

(29) Houston, P. L.; Kable, S. H. *Proc. Natl. Acad. Sci. U.S.A.* **2006**, *103*, 16079.

(30) Goncharov, V.; Herath, N.; Suits, A. G. *J. Phys. Chem. A* **2008**, *112*, 9423.

(31) Shepler, B. C.; Braams, B. J.; Bowman, J. M. *J. Phys. Chem. A* **2007**, *111*, 8282.

(32) Shepler, B. C.; Braams, B. J.; Bowman, J. M. *J. Phys. Chem. A* **2008**, *112*, 9344.

JP810517E